Metabolic engineering of lipid catabolism increases microalgal lipid accumulation without compromising growth

Emily M. Trentacoste[a], Roshan P. Shrestha[a], Sarah R. Smith[a], Corine Glé[a], Aaron C. Hartmann[a], Mark Hildebrand[a], and William H. Gerwick[a,b,1]

[a]Scripps Institution of Oceanography, and [b]Skaggs School of Pharmacy and Pharmaceutical Sciences, University of California, San Diego, La Jolla, CA 92093

Edited by James L. Van Etten, University of Nebraska, Lincoln, NE, and approved October 29, 2013 (received for review May 16, 2013)

Biologically derived fuels are viable alternatives to traditional fossil fuels, and microalgae are a particularly promising source, but improvements are required throughout the production process to increase productivity and reduce cost. Metabolic engineering to increase yields of biofuel-relevant lipids in these organisms without compromising growth is an important aspect of advancing economic feasibility. We report that the targeted knockdown of a multifunctional lipase/phospholipase/acyltransferase increased lipid yields without affecting growth in the diatom *Thalassiosira pseudonana*. Antisense-expressing knockdown strains 1A6 and 1B1 exhibited wild-type–like growth and increased lipid content under both continuous light and alternating light/dark conditions. Strains 1A6 and 1B1, respectively, contained 2.4- and 3.3-fold higher lipid content than wild-type during exponential growth, and 4.1- and 3.2-fold higher lipid content than wild-type after 40 h of silicon starvation. Analyses of fatty acids, lipid classes, and membrane stability in the transgenic strains suggest a role for this enzyme in membrane lipid turnover and lipid homeostasis. These results demonstrate that targeted metabolic manipulations can be used to increase lipid accumulation in eukaryotic microalgae without compromising growth.

metabolism | RNAi | algal biofuel | targeted manipulation | triacylglycerol

The development of alternative fuels is becoming increasingly urgent as the world supply of fossil fuels decreases and atmospheric CO_2 levels continue to rise. Microalgae and cyanobacteria have been identified as promising biological sources of various fuel-relevant molecules including lipids, ethanol, and hydrocarbons (1). Eukaryotic microalgae have received particular recognition due to the ability of many species to accumulate triacylglycerol (TAG), especially under nutrient limitation. These neutral lipids can be converted to fatty acid methyl esters (FAMEs), the main components of biodiesel (2), through transesterification, or refined into other fuel constituents (3). Total lipids and other biomass constituents can be converted into crude oil alternatives through thermochemical processes such as hydrothermal liquefaction (4). The economic feasibility, however, of microalgae as a source of biofuels is dependent upon improvements throughout the production process (5, 6), and one of the most influential improvements would be to increase lipid yields (1, 7). The traditional strain discovery and selection process is one viable approach for finding high-lipid–containing strains (8); however, the recent development of molecular techniques for microalgal strain optimization offers an alternative method to increase lipid production.

To date, engineering efforts for lipid metabolism have focused on increasing lipid biosynthesis or blocking the competing pathways of carbohydrate formation (1). However, of the strategies that have successfully increased lipids, all have resulted in decreased growth in the engineered strains (9–12). Maintaining high growth rates and high biomass accumulation is imperative for algal biofuel production on large economic scales (13), and engineering efforts that increase lipid content without decreasing growth or biomass can significantly reduce production cost and increase the economic viability of algal biofuels (7). Lipid catabolism has largely been ignored as a relevant pathway for engineering, despite being a competing pathway to lipid biogenesis. Lipid breakdown is hypothesized to play roles in quickly providing acyl groups for membrane reorganization as environmental conditions change, contributing to polar lipid synthesis during dark cycles and remobilizing cell membranes upon release from nutrient stress (14, 15).

We hypothesized that the targeted knockdown of lipid catabolism, and specifically lipases, which catalyze the release of free fatty acids (FAs) from lipids, could increase lipid accumulation. We proposed that unlike disrupting carbohydrate pools, which are the primary carbon storage product of many microalgae (16, 17), knockdown of lipid catabolism would have less impact on the primary carbon pathways associated with growth. This work was performed in the diatom *Thalassiosira pseudonana*, a model lipid-accumulating diatom species (18) with an available genome sequence (19). Diatoms have long been attractive sources of biodiesel-type fuels (8, 20), and recent advancements have enabled metabolic engineering in these organisms (21, 22).

Here we report the identification, characterization, and knockdown of *T. pseudonana* genome version 3 protein ID 264297 (Thaps3_264297) in *T. pseudonana* and the screening and characterization of resulting strains. Antisense-containing knockdown strains show no decrease in growth relative to the wild-type (WT) strain, but exhibit increased lipid accumulation during both nutrient-replete and nutrient-limited conditions. These results demonstrate that targeted metabolic manipulations can be used to increase

Significance

As global CO_2 levels rise and fossil fuel abundance decreases, the development of alternative fuels becomes increasingly imperative. Biologically derived fuels, and specifically those from microalgae, are promising sources, but improvements throughout the production process are required to reduce cost. Increasing lipid yields in microalgae without compromising growth has great potential to improve economic feasibility. We report that disrupting lipid catabolism is a practical approach to increase lipid yields in microalgae without affecting growth or biomass. We developed transgenic strains through targeted metabolic engineering that show increased lipid accumulation, biomass, and lipid yields. The target enzyme's ubiquity suggests that this approach can be applied broadly to improve the economic feasibility of algal biofuels in other groups of microalgae.

Author contributions: E.M.T., R.P.S., M.H., and W.H.G. designed research; E.M.T., S.R.S., C.G., and A.C.H. performed research; S.R.S. contributed data and technical support; E.M.T., C.G., A.C.H., M.H., and W.H.G. analyzed data; M.H. and W.H.G. provided technical support; and E.M.T. wrote the paper.

The authors declare no conflict of interest.

This article is a PNAS Direct Submission.

Freely available online through the PNAS open access option.

[1]To whom correspondence should be addressed. E-mail: wgerwick@ucsd.edu.

This article contains supporting information online at www.pnas.org/lookup/suppl/doi:10.1073/pnas.1309299110/-/DCSupplemental.

accumulation of fuel-relevant molecules in eukaryotic microalgae with no negative effects on growth.

Results

Transcriptomics-Guided Identification of Lipase Thaps3_264297. To guide identification of prospective targets for knockdown of lipid catabolism, an Affymetrix whole genome tiling microarray of *T. pseudonana* was analyzed for lipase expression under silicon-limited conditions. Under these conditions, *T. pseudonana* arrests its cell cycle (23) and accumulates TAG, beginning 8 h after nutrient starvation (Fig. 1*A*). Transcript abundances were analyzed over a time series of 4, 8, 12, 18, and 24 h after inoculation into silicon-limited media and compared with abundances at hour 0. Of the genes in *T. pseudonana* containing lipase domains, the gene exhibiting the most consistent decrease in transcript abundance throughout lipid accumulation encoded the predicted hydrolase Thaps3_264297 (Fig. 1*A*). Sequencing of *T. pseudonana* cDNA generated from isolated total RNA revealed a 505-amino-acid (aa), 57-kDa protein product.

Characterization of Thaps3_264297. A BLAST search revealed Thaps3_264297 is a homolog of the human comparative gene identification 58 (CGI-58) protein (29% identity), which is a lipase activator involved in the breakdown of lipid droplets (24) and an acyltransferase thought to facilitate the transfer of acyl groups between storage lipids and phospholipids (25). A multiple sequence alignment of the Thaps3_264297 protein with human CGI-58 and other homologs revealed a conserved His–Gly dipeptide believed to define the boundaries of the lipid-binding pocket (26), a lipase motif GXSXG, characteristic of hydrolytic enzymes including lipases, esterases, and serine proteases (27), and an acyltransferase motif $H(X)_4D$ (27, 28) (Fig. S1*A*). A phylogenetic analysis of Thaps3_264297 and CGI-58 homologs revealed that the enzyme from *T. pseudonana* is more closely related to homologs from yeast, green algae, and plants than to those of vertebrates (Fig. S1*B*). To assess the role of Thaps3_264297 in lipid catabolism, we expressed His6-tagged recombinant Thaps3_264297 protein in *Escherichia coli*. In vitro assays of the purified recombinant protein revealed TAG lipase (Fig. 1*B*), phospholipase (Fig. 1*C*), and lysophosphatidic acid acyltransferase activities (Fig. 1*D*). The known lipase inhibitor tetrahydrolipstatin (Orlistat) inhibited recombinant Thaps3_264297 enzyme activity (Fig. S2). These data indicated Thaps3_264297 is involved in lipid catabolism.

Knockdown of Thaps3_264297 Using Antisense and Interfering RNA. Knockdown of Thaps3_264297 was carried out in *T. pseudonana* using antisense and RNAi approaches. Two constructs, pA78cgi and pI1001cgi, encoding antisense and RNAi, respectively, were designed to a portion of Thaps3_264297 (Fig. S3*A*). Expression of pA78cgi was driven by the fucoxanthin chlorophyll a/b-binding protein (fcp) promoter, whereas pI1001cgi was under the control of an inducible nitrate reductase promoter (21). The constructs were transformed into WT *T. pseudonana* and seven transformants [three antisense strains and four interfering RNA (RNAi) strains] were screened for growth, lipid accumulation under nutrient-replete conditions, and lipid accumulation under nutrient-deplete conditions. All three antisense strains responded similarly, showing comparable growth to WT and increased lipids compared with WT under nutrient-replete and deplete conditions; RNAi strains demonstrated variable results (Fig. S4). Two randomly selected antisense strains (1A6 and 1B1 containing antisense-encoding pA78cgi) and the two RNAi strains (3C2 and 3D6 containing RNAi-encoding pI1001cgi) displaying the best growth were chosen for further characterization and analysis. Knockdown in these four transformants was verified using both immunoblotting (Fig. S3*B*) and functional enzyme assays (Fig. S3*C*).

Strains 1A6 and 1B1 Show Uncompromised Growth. To assess the effects of Thaps3_264297 knockdown on growth and division, we analyzed growth rates and cell densities. Strains 1A6 and 1B1 grew comparably to WT, whereas strains 3C2 and 3D6 exhibited

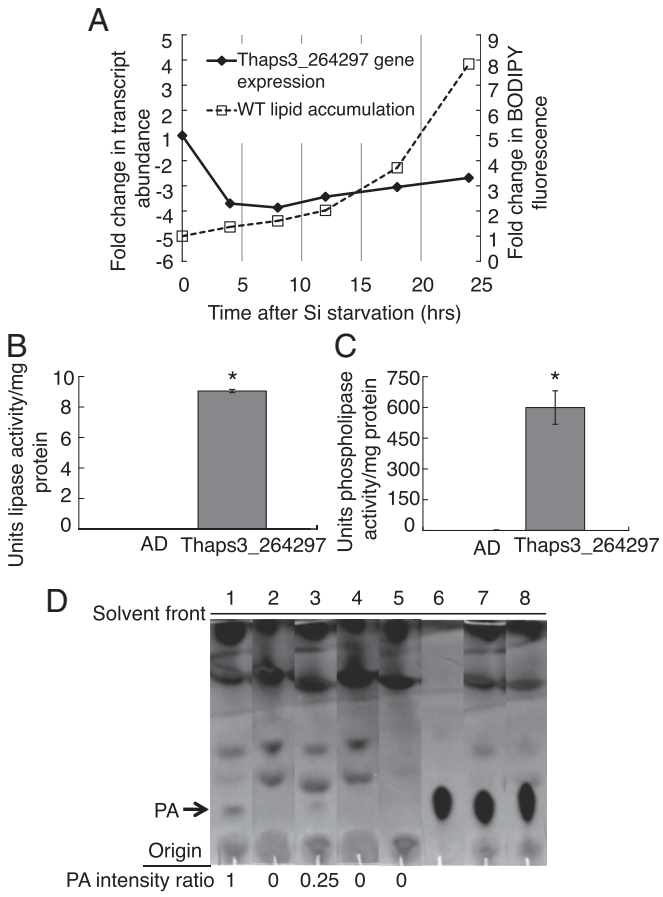

Fig. 1. Identification and characterization of Thaps3_264297. (*A*) Fold change in abundance of Thaps3_264297 transcript (primary axis) during silicon starvation-induced lipid accumulation in WT *T. pseudonana* (secondary axis). Transcriptomic data from a previously generated Affymetrix whole genome tiling microarray was obtained from S.R.S. and M.H. (*B*) Lipase activity compared with negative control alcohol dehydrogenase (AD) ($n = 3$). (*C*) Phospholipase activity compared with negative control AD ($n = 3$). Error bars, SEM. Statistical analyses performed using Student *t* test, $*P < 0.05$. (*D*) Lanes from TLC plate exhibiting lipid extracts from lysophosphatidic acid acyltransferase activity assay reactions using oleoyl-CoA and lysophosphatidic acid as substrates. TLC plate was stained with primuline and analyzed under UV. Activity is demonstrated by production of phosphatidic acid (PA). Reactions consisted of 1, substrates with lysates of *E. coli* expressing recombinant Thaps3_264297; 2, lysates with no substrate; 3, substrates with lysates of *E. coli* expressing an empty control vector; 4, control lysates with no substrates; and 5, substrates with no lysates. Standard PA is shown in 6, cospotted in 7, with extracts from reaction 1 to show comigration, and cospotted in 8, with extracts from reaction 3 to show comigration.

decreased growth with significantly slower doubling times and decreased cell density during stationary phase (Fig. 2*A*). We used the inducible promoter of strain 3C2's RNAi construct to determine that the decrease in growth in this strain is derived from expression of the construct, as the growth rate and cell density of 3C2 in repressive media are not appreciably different from WT (Fig. S5). However, the growth defects of 3C2 and 3D6 do not correlate to the degree of Thaps3_264297 knockdown (Fig. S3 *B* and *C*), indicating that secondary effects of integration, expression, or processing of the RNAi construct may be occurring in these strains—a phenomenon found in plant transformations (29). We also investigated the growth of 1A6 and 1B1 under a 12 h:12 h light:dark regime for 116 h. Strains 1A6 and 1B1 grew comparably to WT under light:dark conditions (Fig. 2*B*), demonstrating similar growth rates to WT during both the light and dark periods (Fig. 2*C*).

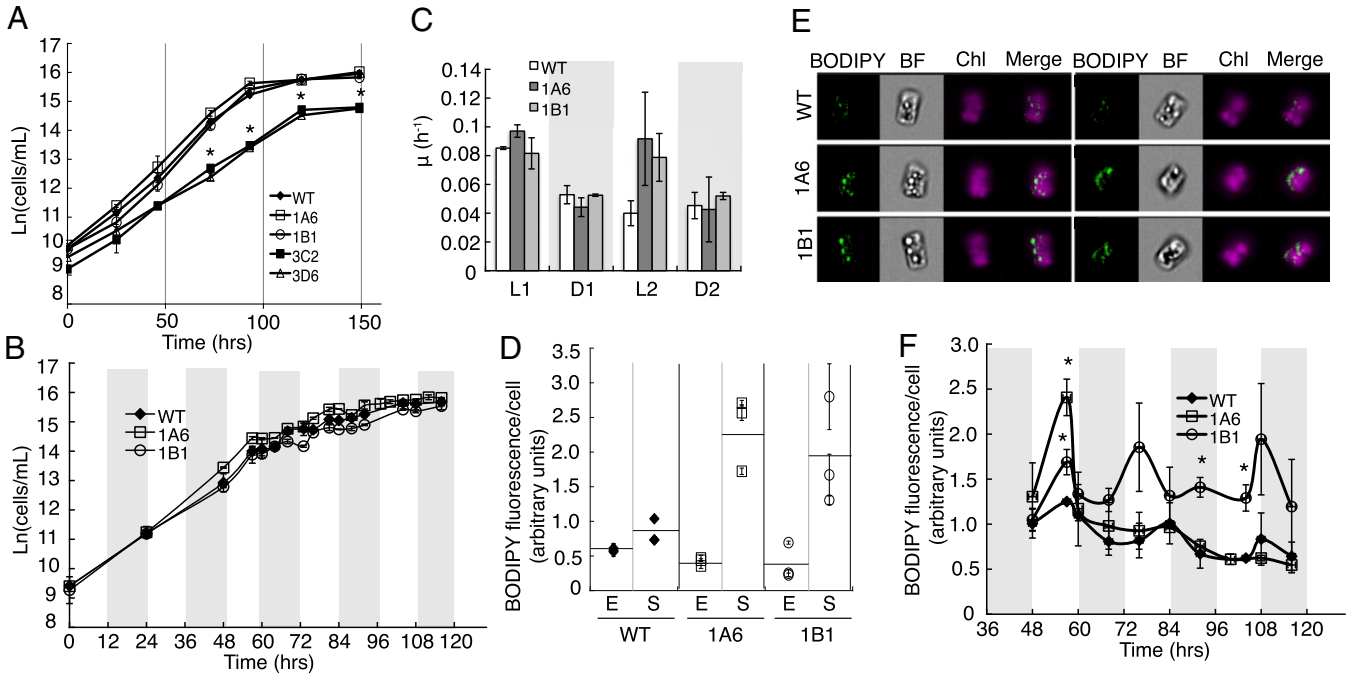

Fig. 2. Characterization of knockdown strains under nutrient-replete conditions. (*A*) Growth of transgenic strains compared with WT as determined by cell density ($n = 3$). (*B*) Growth during 12 h:12 h light:dark cycle as determined by cell density ($n = 2$). Shaded regions denote dark periods. (*C*) Growth rate of transgenic strains compared with WT during light:dark cycle. Shaded regions denote dark periods. L1, first light period; D1, first dark period, etc. (*D*) Increased BODIPY fluorescence and TAG accumulation of 1A6 and 1B1 over WT in stationary phase. E, exponential phase; S, stationary phase. Error bars are SEM from imaging flow cytometry ($n > 100$). Horizontal lines depict average of three graphed populations. (*E*) Imaging flow cytometry images of representative cells selected because their BODIPY fluorescence per cell was the average of the population for three replicates of WT, 1A6, and 1B1 in stationary phase. BODIPY and chlorophyll fluorescence (Chl) are both shown. (*F*) TAG levels in 1A6, 1B1 and WT over light:dark cycle monitored using BODIPY fluorescence. Shaded regions denote dark periods. Error bars are SEM from imaging flow cytometry (n > 100). Statistical analyses were performed using Student *t* test, $*P < 0.05$.

Strains 1A6 and 1B1 Exhibit Increased Lipid Accumulation. To determine if inhibition of Thaps3_264297 affected lipid accumulation, we monitored relative TAG levels in strains not showing compromised growth (1A6 and 1B1) with imaging flow cytometry using the fluorescent neutral lipid dye boron-dipyrromethene (BODIPY) as a proxy (30). Under continuous light conditions, strain 1A6 began accumulating TAG 1 d earlier than WT, and at an accelerated rate (Fig. S6 *A* and *B*). Strains 1A6 and 1B1 contained more TAG per cell in stationary phase than WT (Fig. 2 *D* and *E*) despite similar depletion of TAG stores during exponential phase (Fig. S6*C*). Under a light:dark regime, both 1A6 and 1B1 were able to deplete TAG during dark periods similarly to WT, but both transgenic strains contained higher TAG than WT upon entering the first dark period (Fig. 2*F*). In the latter light periods, WT and 1A6 accumulated less TAG than they depleted, whereas 1B1 continued to accumulate and deplete TAG to consistent levels.

WT *T. pseudonana* accumulates abundant TAG under silicon-limited conditions (18). To test the effect of Thaps3_264297 knockdown on nutrient-starvation–induced TAG accumulation, we compared WT with the transgenic strains 1A6 and 1B1 after transfer into silicon-limited media to induce cell cycle arrest and lipid accumulation. Relative TAG levels were determined and lipid droplet formation was monitored over a time course of 72 h using imaging flow cytometry of cells stained with BODIPY. Strains 1A6 and 1B1 showed significantly increased TAG accumulation per cell compared with WT within 40 h of silicon starvation (Fig. S7 *A* and *B*) and continued to accumulate lipids at a faster rate than WT through 72 h. A high-resolution time series revealed increased lipid accumulation in 1B1 as early as 24 h after silicon starvation (Fig. S7*C*). At 72 h, lipid droplets of 1A6 and 1B1 were larger and more pronounced (Fig. S7*D*).

To compare levels of biofuel-relevant lipids between WT and transgenic strains, total lipids from 1A6, 1B1, and WT were extracted after 0 h of silicon starvation during exponential growth, and after 40 h of silicon starvation. During exponential growth 1A6 and 1B1 contained significantly higher TAG and total lipid content than WT (Fig. 3 *A* and *B*). Because growth is not affected in 1A6 and 1B1, overall lipid yields increased (Fig. S8*A*). An increase in biomass was also observed in 1A6 and 1B1 (Fig. S8*A*). After 40 h of silicon starvation 1A6 and 1B1 contained significantly more TAG and total lipid that WT (Fig. 3 *A*–*C*). TAG content corresponded to BODIPY fluorescence (Fig. S8*B*), suggesting that many of the originally screened transgenic strains also contained increased TAG over WT after silicon starvation.

After 0 and 40 h of silicon starvation, complex lipid species were also extracted from 1A6 and WT and converted to FAMEs for analysis. Fatty acid profiling revealed that quantities of most of the FAME species detected were increased in 1A6, but their relative abundances differed slightly in that levels of 16:0 and 18:2 fatty acids were particularly enriched after 40 h (Fig. 3*D*).

Analysis of Membrane Lipids During Lipid Accumulation. Initial visual observations of silicon-limited cells using imaging flow cytometry revealed increased cellular debris of WT cells over 72 h indicating their degradation—an observation not seen in 1A6 and some other transgenic strains (Fig. S9*A*). Because CGI-58 exhibits phospholipase and acyltransferase activity, we investigated the role of Thaps3_264297 in membrane turnover and the effect of Thaps3_264297 knockdown on cellular membranes. To determine if the visual degradation of cells correlated to damaged or compromised membranes, the nucleic acid stain SYTOX Orange, which passes more easily through compromised membranes, was used to assess relative membrane integrity between WT, 1A6, and 1B1 (31). Under silicon-limited conditions, typically 80% of *T. pseudonana* cells are arrested in G1 phase (23) and contain similar DNA levels, thus differences in SYTOX fluorescence are not attributable to differences in DNA quantity. Strains 1A6 and

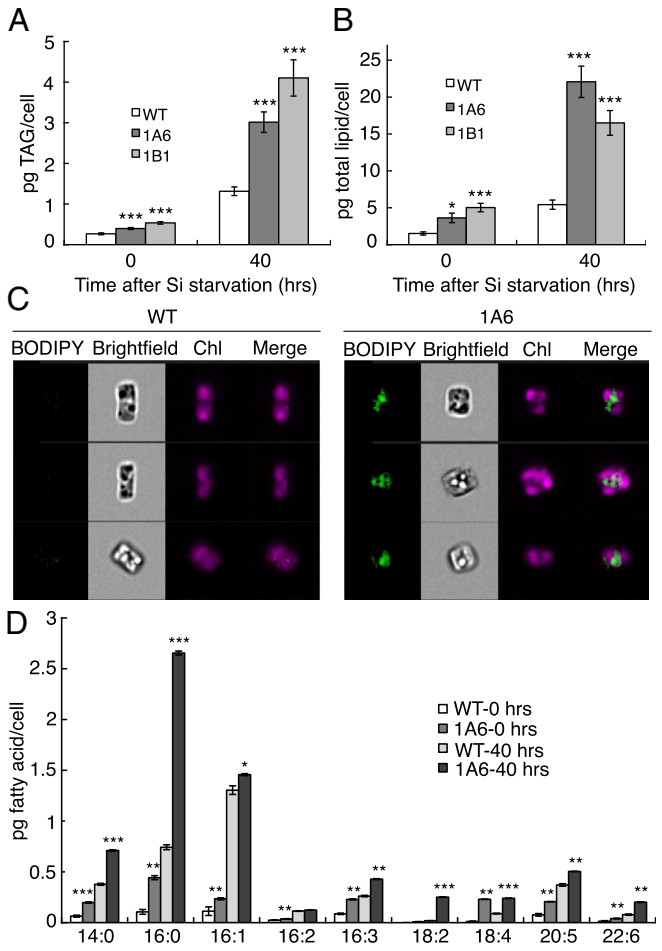

Fig. 3. Increased TAG accumulation in 1A6 and 1B1 during silicon starvation. (*A*) Quantification of picograms of TAG per cell in WT, 1A6, and 1B1 at 0 and 40 h after silicon starvation ($n = 8$). (*B*) Quantification of picograms of total lipid per cell in WT, 1A6, and 1B1 at 0 and 40 h after silicon starvation ($n = 8$). (*C*) Flow cytometry images of representative cells depicting average BODIPY fluorescence of the population for WT and 1A6 after 40 h of silicon starvation. BODIPY and chlorophyll fluorescence (Chl) are both shown. (*D*) FAME profiling of 1A6 and WT during silicon starvation ($n = 2$). Error bars, SEM. Statistical analyses were performed using Student *t* test, $*P < 0.05$, $**P < 0.01$, $***P < 0.001$.

1B1 and WT were subjected to silicon starvation and analyzed after 8 h (when cell cycle arrest occurs and lipid accumulation begins) and 48 h for SYTOX Orange fluorescence using imaging flow cytometry. Whereas both strains showed increased SYTOX Orange fluorescence over time, revealing increased membrane degradation throughout silicon starvation, the WT cells showed significantly more fluorescence per cell relative to 1A6 and 1B1 at both time points, thus indicating less membrane degradation of 1A6 and 1B1 cells (Fig. 4*A* and Fig. S9*B*).

To assess the correlation between SYTOX staining and membrane lipid content, polar lipids were quantified after 40 h of silicon starvation in WT and strains 1A6 and 1B1. Polar lipid content was 4.6-times higher in 1A6 and 3.2-times higher in 1B1 over WT after 40 h, suggesting that polar lipid turnover was also reduced in response to knockdown of Thaps3_264297 (Fig. 4*B*).

We used the inducible promoter of the RNAi construct of 3C2 to further confirm that decreased membrane degradation was a consequence of Thaps3_264297 knockdown. When silicon starvation was carried out under conditions that enabled expression of the RNAi construct, SYTOX fluorescence decreased in 3C2 and increased in WT during the 48 h of silicon starvation. Conversely, when silicon starvation was carried out in repressive media, 3C2 showed an increase in SYTOX fluorescence, indicative of an increase in membrane degradation. (Fig. S9*C*).

Discussion

Metabolic engineering of eukaryotic microalgae to develop improved lipid production strains for algal biofuels has become increasingly feasible with advancements in the understanding of lipid metabolism and the manipulation of microalgal metabolic pathways (1). Only a few attempts have been made to engineer lipid metabolism in microalgae, and to our knowledge, no targeted manipulation to date has significantly increased lipid yields without simultaneously decreasing growth. Although these manipulations have had little success in increasing overall lipid yields, they have shed light on lipid pathway regulation (8, 12, 32). We hypothesized that disrupting lipid catabolism could increase lipid accumulation without negatively affecting growth. Lipid catabolism involves the release of free fatty acids by lipases and the subsequent breakdown of these fatty acids through β-oxidation. It has been ignored as a relevant pathway for targeted manipulation, perhaps because extensive knockout studies in *Arabidopsis thaliana*, which primarily focused on seed oil mobilization, have resulted in numerous mutants of lipid catabolism with impaired growth phenotypes (33). However, because seedling establishment and growth is dependent on lipolysis of stored lipids until the photosynthetic apparatus is formed, one cannot extrapolate these results to microalgae, which go through neither seed nor germination stages.

Although previous transcriptomic analyses in other microalgae found variable expression of annotated lipases during lipid accumulation (34, 35), we expanded our study to include all enzymes containing a lipase motif, such as some hydrolases, and identified a small number of down-regulated enzymes in *T. pseudonana*, including Thaps3_264297 (Fig. 1*A*). Thaps3_264297 is homologous to human CGI-58, which has been shown to be associated with lipid droplets and intimately involved in their breakdown (24). We found Thaps3_264297 to exhibit lipase, phospholipase, and lysophosphatidic acyltransferase activities (Fig. 1 *B–D*), which have also been shown for At4g24160 and Ict1p, CGI-58 homologs in *A. thaliana* and *Saccharomyces cerevisiae*, respectively (36, 37). These activities correspond to the conserved catalytic domains of these enzymes (Fig. S1*A*) and indicate their roles in lipid turnover.

Mutation of CGI-58 in humans causes Chanarin–Dorfman syndrome, a neutral lipid storage disease characterized by excessive accumulation of lipid droplets in cells of various tissues (24). Knockout of the CGI-58 homolog in *A. thaliana* resulted in a Chanarin–Dorfman-like excessive accumulation of lipid droplets in the leaves of the mutant plants; interestingly, these mutant plants did not show any defects in growth or reproduction, suggesting that the CGI-58 homolog was not involved in TAG mobilization of seeds, but rather in maintaining lipid

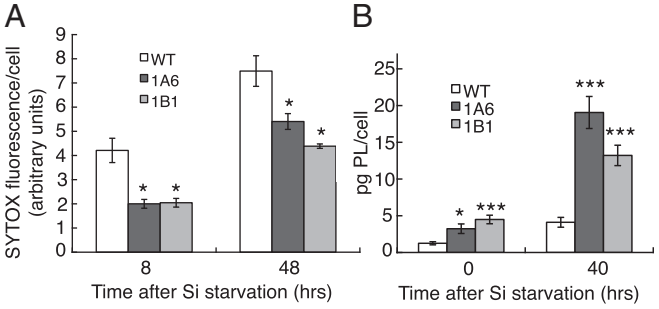

Fig. 4. Increased membrane intactness and polar lipid levels during silicon starvation. (*A*) SYTOX fluorescence per cell in WT, 1A6, and 1B1 at 8 and 40 h of silicon starvation. Error bars are SEM from imaging flow cytometry ($n > 100$). (*B*) Quantification of picograms of polar lipids (PLs) per cell in WT, 1A6, and 1B1 at 0 and 40 h of silicon starvation ($n = 8$). Error bars, SEM. Statistical analyses were performed by Student *t* test, $*P < 0.05$, $***P < 0.001$.

homeostasis in vegetative cells (38). We have similarly shown that knockdown of the CGI-58 homolog in *T. pseudonana* results in increased accumulation of TAG droplets, total lipid production, and lipid yields without negatively affecting growth, cell division, or biomass under continuous light and light:dark cycling (Figs. 2 and 3 and Figs. S6 and S8*A*). Whereas increasing lipid yields is important for economic feasibility, maintaining high growth rates is also imperative for reducing cost of production (13). Additionally, biomass accumulation is a critical factor in current extraction regimes (4), and growth throughout light:dark cycles is necessary for outdoor production. The conserved role of this enzyme across taxa implies that our methods may be applicable to increase lipid yields from other biofuel production strains as well.

We found that during growth, knockdown strains depleted TAG to a similar level as WT and depleted TAG during dark periods, but contained more TAG throughout exponential and stationary phases (Fig. 2 *C–F* and Fig. S6). These results suggest that Thaps3_264297 may not be involved in mobilizing TAG for rapid growth, but rather, like *A. thaliana*'s homolog, in lipid homeostasis or remodeling, therefore allowing the knockdown to grow similarly to WT. This suggests diverse and independent functions for distinct TAG lipases, which is consistent with the variable expression levels of lipases seen in transcriptomic analyses, and demonstrates the importance of such analyses in guiding targeted manipulations. We have shown that knockdown of the CGI-58 homolog in *T. pseudonana* also results in increased polar lipid levels and membrane integrity during silicon starvation (Fig. 4), indicating a role for this enzyme in membrane turnover during nutrient-starvation–induced lipid accumulation and is beneficial to conversion processes such as hydrothermal liquefaction. Knockout of the CGI-58 homolog in *A. thaliana* similarly resulted in an increase in polar lipids (38). It has recently been shown that although 60% of the TAG accumulated under nutrient-limited conditions in the diatom *Phaeodactylum tricornutum* is derived from de novo lipid biosynthesis, substantial turnover of phospholipids also occurs (39). A secondary route to TAG biosynthesis has also been proposed involving intracellular membrane turnover by the enzyme Phospholipid: diacylglclyerol acyltransferase (40, 41). Our SYTOX staining results indicate that plasma membrane phospholipids may also be a source of acyl groups for TAG biosynthesis in WT, and whereas lipid remodeling may normally occur during accumulation, it is disrupted by knockdown of Thaps3_264297.

Lipid pools have been increasingly recognized as dynamic entities with many functions beyond long-term energy storage. Lipid droplets, for example, are known to associate with other organelles (42) and to distribute neutral lipids, phospholipids, lysophospholipids, and acyl groups throughout the cell and between TAG and membranes (43). Our results indicate that the multifunctional lipase, phospholipase, and acyltransferase activities of Thaps3_264297 support a role in maintaining and modifying cellular lipid pools by interacting with these different lipid species. Although disruption of this process does not compromise growth, it drastically affects levels of internal lipid pools, as well as abundances of individual fatty acids (Fig. 3). Buildup of TAG molecules from decreased lipase activity could contribute to the overabundance of 16:0 fatty acids in strain 1A6 after lipid accumulation, as palmitic acid is a prevalent species in *T. pseudonana* neutral lipids (18). Substrate specificity of Thaps3_264297 and the increase in polar lipids in this strain could also contribute to the overabundance of 16:0 and 18:2 seen in 1A6 compared with WT. Further analysis of fatty acid species in individual lipid pools may give insights into the mechanisms behind the skewed fatty acid profile of 1A6.

Our results indicate that disrupting lipid catabolism can be used to produce strains with favorable characteristics for biofuel production. We have shown that knockdown strains yield more lipid than WT under multiple production schemes, including continuous growth as well as nutrient limitation conditions. Although it was not possible for us to assess the performance of the transgenic lines under authentic production conditions, our ability to mimic light:dark conditions supported the concept that at least some of the benefits we documented under controlled laboratory conditions could translate into a production system.

As the ability to engineer algal strains for their fuel molecules progresses, the elucidation of lipid metabolism and its connected pathways becomes increasingly important and relevant. A deeper understanding of carbon flux throughout the full range of cellular processes is necessary to optimize both growth and lipid accumulation in microalgal cultures. Our results demonstrate that lipid catabolism is an integral part of the metabolic processing of lipids throughout cell growth as well as during nutrient starvation and is intimately involved in both lipid homeostasis and accumulation. We have shown that engineering this pathway is a unique and practical approach for increasing lipid yields from eukaryotic microalgae without compromising growth.

Materials and Methods

Strains and Culture Conditions. *T. pseudonana* was grown in batch culture with shaking or stirring and aeration under either continuous illumination or a 12 h:12 h light:dark cycle at 150 $\mu mol \cdot m^{-2} \cdot s^{-1}$ at 18–20 °C in sterile artificial seawater (ASW) medium supplemented with biotin and vitamin B12 at 1 $ng \cdot L^{-1}$ (44). Repressive media contained ammonia as the nitrogen source instead of nitrate (21). To induce silicon starvation, cultures were grown to a midlog phase density of 2×10^6 cells/mL in ASW, pelleted, and washed twice with silicon-free ASW, and then inoculated at 1×10^6 cells/mL into silicon-free ASW in polycarbonate bottles. Silicon starvation experiments were carried out under continuous illumination.

Construction of Vectors, Transformation, and Expression. The vector used to heterologously express Thaps3_264297 in *E. coli* was constructed from the pet298b+ (Novagen) expression vector and expressed in BL21 *E. coli* (Stratagene) using 0.1 mM Isopropyl β-D-1-thiogalactopyranoside. Knockdown vectors pA78cgi and pI1001cgi were constructed using Invitrogen's Multi-Site Gateway Cloning Protocol and transformed into *T. pseudonana* using microparticle bombardment with a Bio-Rad PDS-1000 using established procedures (45), and the presence of integrated constructs was confimed using PCR. Details of vector construction are given in Fig. S3.

Protein Identification, Purification, and Blotting. Soluble proteins were isolated and purified from *E. coli* using nickel-nitrilotriacetic acid resin as described in the Qiagen Expression Handbook. Soluble protein was isolated from *T. pseudonana* by boiling with Laemmli buffer and centrifuging at 4 °C at $10,000 \times g$ for 20 min. Proteins were separated using SDS/PAGE and gels visualized under UV (NuSep). Western blots using Thermo Pierce mouse 6× His primary anti-His tag antibody and Thermo Pierce goat anti-mouse horseradish peroxidase-conjugate secondary antibody were used to detect recombinant protein. Polyclonal antibodies were raised in rabbits against purified recombinant Thaps3_264297 (ProSci) and used to probe *T. pseudonana* lysates with goat anti-rabbit horseradish peroxidase-conjugate secondary antibodies.

Enzymatic Activity Assays. Lipase activity was determined using the QuantiChrom lipase assay kit (BioAssay Systems), using purified *Candida albicans* lipase (Invitrogen) to generate a standard curve and purified alcohol dehydrogenase (Invitrogen) as a negative control. Phospholipase activity was determined using the EnzCheck Phospholipase A2 Assay (Life Technologies). Lysophosphatidic acid acyltransferase activity assays contained 20 μM oleoyl-CoA (VWR International), 100 μM lysophosphatidic acid (Caymen Chemical), and 20 μg cell lysate in reaction buffer (50 mM Tris·HCl, pH 8.0, 300 mM NaCl) and were carried out at room temperature for 30 min and terminated by extracting lipids according to the Bligh–Dyer method (46). Lipids were analyzed by TLC using chloroform:methanol:water (65:25:4) and visualized under UV (302 nm) after staining with primuline. Spots were quantified using the ChemiDoc XRS+ system and Image Lab software (Bio-Rad). Dioleoyl phosphatidic acid (Sigma) was used as a standard for the reaction product.

Imaging Flow Cytometry. Imaging flow cytometry data were collected on an Amnis ImageStreamX at 60× magnification. For SYTOX staining, frozen and fresh cell pellets were tested and found to differ only slightly in response, an order of magnitude less than the relative differences between strains or timepoints; thus, it was determined that frozen pellets could be used for SYTOX analysis. Frozen cell pellets were resuspended in 2.3% (wt/vol) NaCl solution and stained with either 2.3 μg/mL BODIPY for 15 min or 250 nM SYTOX Orange for 20 min, excited with a 488-nm laser at 10 mW, and brightfield and fluorescent images were collected for between 10,000 and 20,000 events. Amnis IDEAS 4.0 software was used to analyze raw image

files. Cutoffs for in-focus and single cells were determined manually, and images were screened to remove cells that were debris.

Lipid Analysis. For lipid analysis, cultures (1 L, ~1×10^6 cells/mL) were centrifuged and rinsed with 0.4 M ammonium formate. Cells were lyophilized, placed under N_2 (g) atmosphere and stored at −80 °C until analysis. Lipids were extracted following the method of Folch et al. (47). Fatty acids were determined by transmethylation using 14% (vol/vol) boron trifluoride/methanol at 70 °C (48). The concentrations of FAMEs were determined with a Hewlett Packard 5890 Series II gas chromatograph equipped with a flame ionization detector (FID). FAMEs were identified by comparison of retention times to authentic lipid standards (68A and 68D, Nu-Check Prep). Quantification of C14–C18 and C20–C24 fatty acids was performed relative to known concentrations and FID peak areas of C13 and C19 FAME internal standards, respectively. The fatty acid methylation reaction efficiency was determined from the C15 FA internal standard added to each lyophilized algal pellet.

Lipid class composition was determined using the method of Carilli et al. (49). Crude lipid extracts were fully dried under nitrogen gas and resuspended in 500 μL of chloroform. Immediately following, 1 μL of sample was spotted on each of six silica-coated quartz Chromarods (S-III; Iatron Laboratories, Inc.). After spotting, the crude lipid extracts were separated into lipid classes by first developing for 25 min in hexane:diethyl ether:acetic acid (99:1:0.05) (v:v:v), drying at ~100 °C for 4 min, then developing in hexane:diethyl ether:acetic acid (80:20:0.1) (v:v:v) for 25 min and drying again. Chromatograms were generated for each rod using FID via an Iatroscan TLC-FID MK-5 (Iatron Laboratories, Inc.) and LabView software (National Instruments). The concentration of each lipid class was calculated using retention times of known standards.

ACKNOWLEDGMENTS. We thank L. Gerwick and N. Engene (University of California, San Diego) for technical advice and M. Ohman for the Iatroscan. E.M.T. is supported by National Institutes of Health Marine Biotechnology Training Grant Fellowship 5T32GM067550. We acknowledge support by the California Energy Commission's "California Initiative for Large Molecule Sustainable Fuels," Agreement No. 500-10-039 and additional support (to M.H.) from the Air Force Office of Scientific Research Grants FA9550-08-1-0178 and FA9550-08-1-0178, Department of Energy Grants DE-EE0001222 and DE-EE0003373, and National Science Foundation Grant CBET-0903712.

1. Radakovits R, Jinkerson RE, Darzins A, Posewitz MC (2010) Genetic engineering of algae for enhanced biofuel production. *Eukaryot Cell* 9(4):486–501.
2. Hossain S, Salleh A, Boyce AN, Chowdhury P, Naqiuddin M (2008) Biodiesel fuel production from algae as renewable energy. *Am J Biochem Biotechnol* 4(3):250–254.
3. Pienkos PT, Darzins A (2009) The promise and challenges of microalgal-derived biofuels. *Biofuel Bioprod Bior* 3(4):431–440.
4. Barreiro DL, Prins W, Ronsse F, Brilman W (2013) Hydrothermal liquefaction (HTL) of microalgae for biofuel production: State of the art review and future prospects. *Biomass Bioenerg* 53:113–127.
5. Coates RC, Trentacoste EM, Gerwick WH (2013) Bioactive and novel chemicals from microalgae. *Handbook of Microalgal Culture*, eds Richmond A, Hu Q (Wiley-Blackwell, Oxford), Ed 2, pp 504–531.
6. Waltz E (2013) Algal biofuels questioned. *Nat Biotechnol* 31:12.
7. Davis R, Aden A, Pienkos PT (2011) Techno-economic analysis of autotrophic microalgae for fuel production. *Appl Energy* 88(10):3524–3531.
8. Sheehan J, Dunahay TG, Benemann J, Roessler PG (1998) A look back at the US Department of Energy's Aquatic Species Program: Biodiesel from algae. Report No. NREL/TP-580-24190 (National Renewable Energy Laboratory, Golden, CO).
9. Wang ZT, Ullrich N, Joo S, Waffenschmidt S, Goodenough U (2009) Algal lipid bodies: Stress induction, purification, and biochemical characterization in wild-type and starchless *Chlamydomonas reinhardtii*. *Eukaryot Cell* 8(12):1856–1868.
10. Li Y, Han D, Hu G, Sommerfeld M, Hu Q (2010) Inhibition of starch synthesis results in overproduction of lipids in *Chlamydomonas reinhardtii*. *Biotechnol Bioeng* 107(2): 258–268.
11. Work VH, et al. (2010) Increased lipid accumulation in the Chlamydomonas reinhardtii sta7-10 starchless isoamylase mutant and increased carbohydrate synthesis in complemented strains. *Eukaryot Cell* 9(8):1251–1261.
12. Radakovits R, Eduafo PM, Posewitz MC (2011) Genetic engineering of fatty acid chain length in *Phaeodactylum tricornutum*. *Metab Eng* 13(1):89–95.
13. Borowitzka MA (1992) Algal biotechnology products and process: Matching science and economics. *J Appl Phycol* 4(3):267–279.
14. Solovchenko AE (2012) Physiological role of neutral lipid accumulation in eukaryotic microalgae under stresses. *Russ J Plant Physiol* 59(2):167–176.
15. Guschina IA, Harwood JL (2009) *Lipids in Aquatic Systems*, eds Kainz M, Brett MT, Arts MT (Springer Science, New York), pp 1–24.
16. Chauton MS, Winge P, Brembu T, Vadstein O, Bones AM (2013) Gene regulation of carbon fixation, storage, and utilization in the diatom *Phaeodactylum tricornutum* acclimated to light/dark cycles. *Plant Physiol* 161(2):1034–1048.
17. Li Y, Han D, Sommerfeld M, Hu Q (2011) Photosynthetic carbon partitioning and lipid production in the oleaginous microalga *Pseudochlorococcum* sp. (Chlorophyceae) under nitrogen-limited conditions. *Bioresour Technol* 102(1):123–129.
18. Yu E, et al. (2009) Triacylgycerol accumulation and profiling in the model diatoms *Thalassiosira pseudonana* and *Phaeodactylum tricornutum* (Baccilariophyceae) during starvation. *J Appl Phycol* 21(6):669–681.
19. Armbrust EV, et al. (2004) The genome of the diatom *Thalassiosira pseudonana*: Ecology, evolution, and metabolism. *Science* 306(5693):79–86.
20. Hildebrand M, Davis AK, Smith SR, Traller JC, Abbriano R (2012) The place of diatoms in the biofuels industry. *Biofuels* 3(2):221–240.
21. Poulsen N, Chesley PM, Kroger N (2006) Molecular genetic manipulation of the diatom *Thalassiosira pseudonana* (Bacillariophyceae). *J Phycol* 42(5):1059–1065.
22. De Riso V, et al. (2009) Gene silencing in the marine diatom *Phaeodactylum tricornutum*. *Nucleic Acids Res* 37(14):e96.
23. Hildebrand M, Frigeri LG, Davis A (2007) Synchronized growth of *Thalassiosira pseudonana* (Bacillariophyceae) provides novel insights into cell-wall synthesis processes in relation to the cell cycle. *J Phycol* 43(4):730–740.
24. Yamaguchi T, Osumi T (2009) Chanarin-Dorfman syndrome: Deficiency in CGI-58, a lipid droplet-bound coactivator of lipase. *Biochim Biophys Acta* 1791(6):519–523.
25. Montero-Moran G, et al. (2010) CGI-58/ABHD5 is a coenzyme A-dependent lysophosphatidic acid acyltransferase. *J Lipid Res* 51(4):709–719.
26. Schrag JD, Cygler M (1997) Lipases and alpha/beta hydrolase fold. *Methods Enzymol* 284:85–107.
27. Cygler M, et al. (1993) Relationship between sequence conservation and three-dimensional structure in a large family of esterases, lipases, and related proteins. *Protein Sci* 2(3):366–382.
28. Heath RJ, Rock CO (1998) A conserved histidine is essential for glycerolipid acyltransferase catalysis. *J Bacteriol* 180(6):1425–1430.
29. Filipecki M, Malepszy S (2006) Unintended consequences of plant transformation: A molecular insight. *J Appl Genet* 47(4):277–286.
30. Xu D, et al. (2013) Detection and quantitation of lipid in the microalga *Tetraselmis subcordiformis* (Wille) Butcher with BODIPY 505/515 staining. *Bioresour Technol* 127: 386–390.
31. Gerken HG, Donohoe B, Knoshaug EP (2013) Enzymatic cell wall degradation of *Chlorella vulgaris* and other microalgae for biofuels production. *Planta* 237(1):239–253.
32. Moellering ER, Benning C (2010) RNA interference silencing of a major lipid droplet protein affects lipid droplet size in *Chlamydomonas reinhardtii*. *Eukaryot Cell* 9(1):97–106.
33. Graham IA (2008) Seed storage oil mobilization. *Annu Rev Plant Biol* 59:115–142.
34. Miller R, et al. (2010) Changes in transcript abundance in *Chlamydomonas reinhardtii* following nitrogen deprivation predict diversion of metabolism. *Plant Physiol* 154(4): 1737–1752.
35. Rismani-Yazdi H, Haznedaroglu BZ, Hsin C, Peccia J (2012) Transcriptomic analysis of the oleaginous microalga *Neochloris oleoabundans* reveals metabolic insights into triacylglyceride accumulation. *Biotechnol Biofuels* 5(1):74.
36. Ghosh AK, Ramakrishnan G, Rajasekharan R (2008) YLR099C (ICT1) encodes a soluble Acyl-CoA-dependent lysophosphatidic acid acyltransferase responsible for enhanced phospholipid synthesis on organic solvent stress in *Saccharomyces cerevisiae*. *J Biol Chem* 283(15):9768–9775.
37. Ghosh AK, Chauhan N, Rajakumari S, Daum G, Rajasekharan R (2009) At4g24160, a soluble acyl-coenzyme A-dependent lysophosphatidic acid acyltransferase. *Plant Physiol* 151(2):869–881.
38. James CN, et al. (2010) Disruption of the *Arabidopsis* CGI-58 homologue produces Chanarin-Dorfman-like lipid droplet accumulation in plants. *Proc Natl Acad Sci USA* 107(41):17833–17838.
39. Burrows EH, et al. (2012) Dynamics of lipid biosynthesis and redistribution in the marine diatom *Phaeodactylum tricornutum* under nitrate deprivation. *Bioenerg Res* 5(4):876–885.
40. Boyle NR, et al. (2012) Three acyltransferases and nitrogen-responsive regulator are implicated in nitrogen starvation-induced triacylglycerol accumulation in *Chlamydomonas*. *J Biol Chem* 287(19):15811–15825.
41. Yoon K, Han D, Li Y, Sommerfeld M, Hu Q (2012) Phospholipid:diacylglycerol acyltransferase is a multifunctional enzyme involved in membrane lipid turnover and degradation while synthesizing triacylglycerol in the unicellular green microalga *Chlamydomonas reinhardtii*. *Plant Cell* 24(9):3708–3724.
42. Goodman JM (2008) The gregarious lipid droplet. *J Biol Chem* 283(42):28005–28009.
43. Zehmer JK, et al. (2009) A role for lipid droplets in inter-membrane lipid traffic. *Proteomics* 9(4):914–921.
44. Darley WM, Volcani BE (1969) Role of silicon in diatom metabolism. A silicon requirement for deoxyribonucleic acid synthesis in the diatom Cylindrotheca fusiformis Reimann and Lewin. *Exp Cell Res* 58(2):334–342.
45. Dunahay TG, Jarvis EE, Roessler PG (1995) Genetic transformation of the diatoms *Cyclotella cryptica* and *Navicula saprophila*. *J Phycol* 31(6):1004–1012.
46. Bligh EG, Dyer WJ (1959) A rapid method of total lipid extraction and purification. *Can J Biochem Physiol* 37(8):911–917.
47. Folch J, Lees M, Sloane Stanley GH (1957) A simple method for the isolation and purification of total lipides from animal tissues. *J Biol Chem* 226(1):497–509.
48. Christie WW (2003) *Lipid Analysis: Isolation, Separation, Identification and Structural Analysis of Lipids* (The Oily Press, PJ Barnes & Associates, Bridgewater, UK), Ed 3.
49. Carilli J, Donner SD, Hartmann AC (2012) Historical temperature variability affects coral response to heat stress. *PLoS ONE* 7(3):e34418.